

# **Low-Temperature Thermochronometry of the Avawatz Mountains; Implications for the Eastern Terminus and Inception of the Garlock Fault Zone**

-Logan Daniel Chinn

## **Abstract:**

Located at the nexus of three tectonic regimes and the eastern terminus of the Garlock fault zone, the Avawatz Mountains are an actively uplifting range that is host to young (Pleistocene - Holocene) crustal shortening. Vertical displacement along reverse structures in the Avawatz Mountains has been linked to motion along the Garlock fault zone (McGill & Sieh, 1991). In this study I use apatite helium and apatite fission-track cooling ages from the Avawatz Mountains to establish the exhumation history of the eastern terminus of the Garlock fault zone, and to investigate the timing of vertical displacement along the fault zone's eastern-most branch – the Mule Spring fault. Extant cooling ages (Reinert, 2004) are modeled, and found to indicate an increase in cooling rate between 11-9 Ma, when rates transitioned from  $\sim 3$  °C/Ma to  $\sim 6$  °C/Ma (0.1 km/Ma to 0.2 km/Ma exhumation rates, respectively). As uplift in this range is hypothesized to be related to the Garlock, this 11-9 Ma increase in cooling rate is interpreted to record the inception age of the Garlock, and is in agreement with more recent estimates. Furthermore, young cooling ages in the foothills of the Avawatz

indicate additional structures may exist along which the range has been uplifted and exhumed. New thermochronometric cooling ages reveal the timing of vertical displacement along the Mule Spring fault in the western Avawatz to be ~3 Ma, yet this displacement of cooling ages across the Mule Spring fault is not observed in the east of the range. However, additional structures in the hanging-wall of the Mule Spring fault do indicate vertical displacement. Young footwall ages indicate the Avawatz Mountains and Mule Spring fault are being uplifted and exhumed along another structure(s), potentially located in the Avawatz foothills or hidden beneath the expansive bajada.

### **Introduction:**

The Avawatz Mountains are a prominent mountain range located in the northeastern corner of the Mojave tectonic province, at the junction of the sinistral Garlock fault zone and dextral southern Death Valley fault zone (Figure 1). Uplift of the Avawatz Mountains is unusual in that it occurs at nexus of three tectonic regimes: Basin and Range extension to the north, dextral shearing of the Eastern California Shear Zone to the east, and the subdued topography and strike-slip regime of the Mojave block to the south. Previous studies (e.g., Spencer, 1991a, 1991b; Brady & Troxel, 1981, Brady, 1986) attributed the uplift of the range to vertical motion along the easternmost branch of the Garlock fault zone; on the basis of the mapped termination of the Mule Spring fault as a thrust (Figure 2). McGill and Sieh (1991) even noted that the vertical displacement of offset geomorphic features of the Garlock fault on the northern flank of the Avawatz Mountains is ~13% of the left-lateral offset. Although the Avawatz Mountains are thought to record strain from the eastern terminus of the Garlock, the

timing of vertical displacement along contractional structures, as well as the apparent rates of exhumation of the range, requires further investigation.

The purpose of this study is to determine the history of uplift and exhumation of the Avawatz Mountains, and to investigate the structures that have resulted in the vertical displacement that has formed the range as we see it today. As the Avawatz Mountains are bound by the Garlock fault zone (Figure 2), studying the exhumation history of the range may yield insight into the age of inception of the Garlock. Furthermore, the exhumational history across the range-bounding Mule Spring fault can also confirm the presence and timing of vertical displacement along this structure. I used low-temperature thermochronometry to determine the timing and rates of apparent exhumation of the range, and establish the presence of vertical displacement across the Mule Spring fault. Thermochronometric data from a previous study (Reinert, 2004) are re-examined and modeled, and new data from across the Mule Spring fault are presented. New conclusions are then drawn about the timing of uplift and exhumation of the range, which structures account for the uplift, as well as the inception age of the Garlock fault zone. From these conclusions, speculations are then made about the structural evolution concerning the Garlock and southern Death Valley fault zones.

### **Geologic Background:**

#### ***Garlock fault zone***

The Garlock fault zone (GFZ), which extends ~260 km across southern California, is one of the principal onshore Holocene faults of the western United States (Figure 1). The inception age of this fault is not well constrained, but there is increasing

evidence for a younger age of inception than previously thought. Smith (1962; Smith & Ketner, 1970) placed the age of inception during Miocene time, based on the offset of the Independence dike swarm and the Eagle Crags volcanic field, which also yield the maximum recorded offset of 64 km. Monastero et al (1997), placed the initiation at post-17 Ma (mid-Miocene), based on offset of the Cudahy Camp formation in El Paso basin. Smith (2002) used offset volcanics of the Lava Mountains to project the age of inception to 16.4 Ma, accounting for the full 64 km offset of the Independence dike swarm. Burbank and Whistler (1987) attributed rotation of El Paso basin sedimentary units to sinistral movement on the Garlock, placing the initiation between 10-7 Ma. Loomis and Burbank (1988) later constrained this timing even further to 10-9 Ma based on offset volcanic and sedimentary units of the Ricardo Group in El Paso basin. Blythe and Longinotti attributed an increase in exhumation rate from AFT analyses of samples from the Tehachapi Mountains to infer a ~10 Ma inception. Thus, there is increasing evidence for inception of the Garlock fault zone occurring after 10 Ma.

Bryant (2000) compiled average slip rates between 11 mm/yr in the western segment of the Garlock to 1 mm/yr in the eastern segment, with an overall average slip rate of 7 mm/yr. McGill and Sieh (1991) estimated a slip rate of ~3 mm/yr for the eastern Garlock, with an earthquake recurrence interval of 300-2000 yrs. The total accumulated slip is known to decrease from west to east towards a hypothetical zone of zero displacement projected east of the Avawatz (Davis and Burchfiel, 1973, Troxel et al., 1972). The eastern terminus of the Garlock fault zone consists of three active (Holocene) branches –the Leach Lake fault, Arrastre Spring fault, and the Mule Spring - Old Mormon Spring fault(s). The Avawatz Mountains are bound to the north by the

sinistral oblique-slip Mule Spring fault, which continues to the east as the Old Mormon Spring reverse fault. For the purpose of this study, the Mule Spring - Old Mormon Spring faults will herein only be referred to as the Mule Spring fault, as they are interpreted as continuations of the same structure.

As the Mule Spring fault wraps southeastwardly around the Avawatz Mountains, it is mapped as a thrust fault (Spencer, 1990b, Troxel & Butler, 1971 field mapping). The large difference in topographic relief across the Mule Spring fault leads one to believe that the structure may be responsible for the majority of mountain uplift; however very few researchers have attempted to quantify the timing of uplift and exhumation (e.g., Brady, 1984; Spencer, 1990a, Reinert, 2004), or confirm the sense of vertical displacement along this structure. Thus, understanding how the Garlock terminates, and the timing of its displacement is important to our knowledge of the structural evolution of the range.

Assessing the sense and timing of slip along the Mule Spring fault is challenged by a lack of reference horizons to compare across the fault, and this is due to the generally crystalline nature of rock types in the Avawatz massif. The dominant rock types of the Avawatz Mountains include Mesozoic magmatic arc granitoids and lesser Precambrian – Paleozoic metasedimentary units (Spencer, 1990b). In contrast, the bedrock of the Avawatz foothills includes granodiorite, Precambrian gneiss and granite, Proterozoic Crystal Springs and Kingston Peak formations of the Pahrump group, Tertiary metasedimentary units, and evaporate-rich Tertiary sediments from the nearby Noble Hills, as well as numerous Pleistocene – Holocene alluvial-fan and debris-flow complexes. Thus, there are no originally horizontal sedimentary units or geomorphic

markers in the Avawatz Mountains that once crossed the Mule Spring and have since been offset.

### ***Southern Death Valley fault zone***

The Mule Spring fault is the boundary that separates the high relief of the Avawatz Mountains massif from the low-lying foothills to the north, and these foothills are subsequently separated from the low-lying depositional basins by branches of the southern Death Valley fault zone. The southern Death Valley fault zone (SDV), first recognized by Noble (1941), comprises dextral-slip faults that extend southeast from Cinder Hill towards the Garlock fault zone (Machette & Pietty, 2001). Part of the Death Valley fault system, the SDV is the southern section of four total fault systems (i.e., Fish Lake, Northern Death Valley, Black Mountains, Southern Death Valley). It has been long proposed (Burchfiel & Stewart, 1966) that displacement of the Death Valley fault system has resulted in extension that has formed the Death Valley half-graben, as part of a pull-apart basin. Neogene to Quaternary volcanic and sedimentary units have been offset throughout the southern Death Valley area. Estimates of total dextral displacement of younger (Quaternary) sediment is on the order of ~8 km, whereas older rocks are offset ~50 km (Machette & Pietty, 2001). The southern Death Valley fault zone can be traced to the southeast towards its intersection with the Garlock fault zone.

Upon intersection with the Garlock, the southern Death Valley fault zone changes its strike to wrap around the Avawatz foothills. At this location there may be a younger reverse component of slip on some strands of the fault zone (Machette & Pietty, 2001). Holocene activity on two main strands of the SDV near the Confidence Hills appears to

die-out near the Noble Hills (Figure 1), northwest of the Avawatz Mountains. However, additional traces with Quaternary displacement extend to the Garlock fault zone (Machette & Piety, 2001). The southern end of the SDV is poorly defined, and efforts to map it in detail (1:24,000) remain unpublished (Troxel and Butler, 1971 field mapping). However, Quaternary slip is expressed as far south as the fault's intersection with the Garlock (Butler, 1984; Brady, 1986), and the fault zone may even extend further to the Bristol and Old Dad Mountains (Brady, 1988). Menges et al. (2005) concluded that young deformation in the southern Death Valley region includes a contractional component, likely related to the Eastern California Shear Zone. The dip of the SDV is inferred to be near vertical based on the fault's linear surface trace (e.g. Burchfiel and Stewart, 1966; Butler, 1984), yet as it approaches the Garlock fault zone the SDV appears to be bent and has younger reverse motion (Butler, 1984). Brady (1986) noted that the Pleistocene alluvial fans on the eastern and northern sides of the Avawatz have been deformed, uplifted, and deeply dissected – attributing these characteristics to uplift of the Avawatz, during or shortly after deposition of the alluvial fan complex. Although a number of measurements of Quaternary offset along the SDV have been recorded (e.g., Wills, 1989; Brady, 1986; Piety, 1995) there are no definitive age/offset data to compute slip rates along the southern portion of the SDV. However, because of Holocene offset and consideration of slip rates in the nearby Black Mountain fault zone to the north, the SDV is considered to have a tentative slip rate of 1-5 mm/yr (Machette & Piety, 2001).

### ***Young deformation in the Avawatz foothills***

Several geologic and topographic features indicate that uplift along south-dipping reverse faults continues into the Quaternary; however little is known about vertical displacement on these structures before the Quaternary. Troxel and Butler (1998) and Brady (1986) mapped the trace of the Mule Spring fault for ~20 km and interpreted the fault to be a south-dipping thrust. This mountain range is flanked to the north and east by an expansive bajada, formed by the well-preserved Pleistocene to Holocene alluvial-fan and debris-flow complexes (Menges, 2007). These fans stem from the northern extent of the Avawatz foothills, where blind thrusting along strike of the northern branch of the southern Death Valley fault zone is thought to have folded the overlying Pleistocene alluvial fans (Menges, 2007; Green et al, 2007; Mendonça, 2006, 2007). The uplift of the Avawatz foothills, possibly related to folding of these fans, has resulted in an alluvial strath unconformity (Figures 3, 4) on terraces throughout the foothills. Thrusting in the northern foothills has emplaced bedrock over alluvium, as well as uplifted previously faulted alluvial fans (Menges, 2007). A two meter high thrust scarp below the Mule Spring fault (near Old Mormon Spring) also offsets an alluvial fan relatively dated to ~10 ka, based on comparing the degree of desert pavement to that of a local fan of known age (Stroud and McGill, 1994a, Calzia and Rämö, 2000). Here the fault emplaces Mesozoic granitic rocks and Paleozoic to Precambrian sedimentary bedrock over Quaternary debris-flow fans (Spencer, 1990a; Spencer, 1990b; Stroud and McGill, 1994a; Stroud and McGill, 1994b).

Parts of the Mule Spring fault zone, up to a kilometer wide, consist of vertical slivers of brecciated bedrock. Many stranded alluvial fans rest unconformably on fault rocks - sediment consisting entirely of grus derived from granitic bedrock along the

range front. The apices of these fans have been laterally displaced at least several meters from their source, probably by oblique reverse slip on a discrete strand of the Mule Spring thrust. Additionally, the folding and tilting of Miocene sediments in the interior of the range (Brady, 1984; Spencer, 1990a), and the presence of Pliocene lake sediments on top of the range over a kilometer above the active depositional basin (Brady, 1984), indicate significant post-Miocene crustal shortening. This relatively young shortening and stark topographic relief bounding the depositional basins indicate that transpression has played an important role in the development of the eastern terminus of the Garlock fault zone. By studying the history of vertical displacement along contractional structures related to the Garlock fault zone in the Avawatz Mountains, insight can be gained about the role the Garlock plays in the uplift and exhumation of the range and the younger uplift of the foothills.

### **Methods and Approach:**

The two questions this research aims to address are: 1) What is the exhumational history of the Avawatz massif, and 2) What can the cooling history across the range-bounding Mule Spring fault tell us about vertical displacement on this fault. The dominantly intrusive and metamorphic nature of rock types in the Avawatz Mountains, and the resulting absence of reference horizons, challenge our ability to establish the history of thrust-related exhumation based on structural observations alone. For this reason I utilize low-temperature thermochronometry, which is particularly useful in establishing the exhumation history of rock types typical of the Avawatz Mountains.

## ***Technique***

The thermal sensitivity and low closure temperatures of AHe and AFT make these thermochronometers particularly useful indicators of small magnitudes of accelerated exhumation in the shallow (1-5 km) crust, which may be produced by fault displacements. These methods have been used to successfully deduce the extent, rate and timing of motion on faults (e.g. Stockli et al, 2000, Ehlers et al., 2002). In this study, we utilize apatite (U-Th)/He (AHe) and apatite fission-track (AFT) cooling ages from predominately Mesozoic magmatic arc granitoids (Spencer, 1990b) in order to address our questions concerning the Avawatz Mountains and the range-bounding Mule Spring fault.

Apatite helium thermochronometry is based on the production of  $^4\text{He}$  in the crystal lattice from the decay of  $^{238}\text{U}$ ,  $^{235}\text{U}$ ,  $^{232}\text{Th}$ , and  $^{147}\text{Sm}$ , and that the amount of  $^4\text{He}$  retained in the crystal lattice is based on the ambient temperature and diffusivity of Helium (Zeitler, 1987, Wolf, 1996). The closure temperature of apatite helium, used to interpret cooling ages, ranges from ~55-75 °C (e.g. Wolf, 1996; Warnock, 1997; Farley, 2000, Flowers, 2009). Apatite fission-track thermochronometry utilizes linear zones of damage in crystals formed by the spontaneous fission of  $^{238}\text{U}$  (Fleischer et al., 1975). The stability of these tracks, similar to helium retention in apatite, is based on the ambient temperature. The closure temperature commonly used for AFT interpretation is ~100-120 °C (Gleadow and Duddly, 1981, Ketcham et al., 2007). These closure temperatures vary, depending predominately on the rate of cooling, grain size, and radiation damage (Dodson, 1973; Shuster & Farley, 2009; Flowers, 2009).

## ***Sampling Strategy***

Data for this study come from two separate sampling transects, each addressing different portions of our research questions. To determine the apparent exhumation rate of the Avawatz massif, data from ten samples along a steep topographic transect (10 AHe ages, 5 AFT ages, Figures 2, 5, 6) from a previous study (Reinert, 2004) were re-examined and forward modeled using HeFTy (Ketchum, 2005) (e.g., Clark et al., 2010; Lease et al 2011; Duvall et al. 2013). The total elevation difference for these samples spans 850 m over a 7 km long transect (Figure 6). Additionally, to determine and compare the cooling history across the Mule Spring fault, ten samples (4 AHe ages, 10 AFT) from a lateral transect (Figure 7) were collected and analyzed. These samples were collected 10 km west of the steep topographic transect, just east of where the Mule Spring fault intersects the southern Death Valley fault zone, as the Mule Spring begins to wrap southwardly around the range. Cooling ages from across the fault were compared to determine whether vertical displacement has occurred along the Mule Spring since these samples cooled below their AHe and AFT closure temperatures. Elevation varies by only ~160 m over the 2.5 km distance of this sample suite.

Samples from the steep topographic profile, which were collected from two adjacent ridges, are projected onto a single plane for the purpose of the elevation profile (Figures 6, 8, and 9). Due to a lack of reference horizons in the hanging wall of the Mule Spring fault, cooling ages can not be analyzed as a depth profiles (Clark et al., 2010). Given this absence of a physical reference horizon to measure depth from, apparent exhumation rates of the Avawatz can only be estimated by plotting sample age versus elevation. However, rather than estimating rates by applying linear trends to

cooling ages, the cooling history of these samples are instead forward modeled. Three assumptions used are: (1) a flat closure isotherm at the time of closure, not bent by topography (2) at a given time, samples had a spatially uniform erosion rate, and (3) that the closure isotherm has remained at a constant depth, allowing a samples cooling history to represent movement relative to the surface (Reiners and Brandon, 2006).

### ***Sample Analyses***

All samples were mechanically crushed and separated using standard magnetic and heavy liquid techniques, either in-house at the University of Washington or by Apatite to Zircon, Inc. Apatite helium ages from Reinert, 2004, were obtained at the Reiners (U-Th)/He Chronometry Lab at Yale University, CT, and corrected for alpha ejection (Farley et al., 1996). Individual apatite grains were measured and repeated in triplicates for most samples to ensure reproducibility. New Apatite helium ages were analyzed in the Flowers lab at University of Colorado, Boulder, and corrected for alpha ejection (Farley, 1996). For these samples 5 grains were measured to ensure reproducibility. Apatite fission-track dates from Reinert (2004) were obtained at the fission-track laboratory facility at the University of Washington by the late Richard Stewart. Apatite grains were mounted in epoxy, polished and etched with 5.0M HNO<sub>3</sub> for 20 seconds according to Wagner and Van den Haute (1992). Samples were then covered with mica detectors and sent to the Oregon State Reactor Facility to be irradiated for 25 hours. Mica detectors were then etched in 40% HF for 20 minutes. New Apatite fission-track ages were determined by Ann Blythe and Anne Fendick at Occidental College, Los Angeles. Apatite grains from these samples were mounted in epoxy and etched in 5.5M HNO<sub>3</sub> at 18°C for 22 seconds. An external muscovite

detector was attached to each sample, which were then irradiated in the Oregon State Reactor Facility. Following irradiation, muscovite detectors were etched in 48% HF at 18°C for 30 minutes. All ages are central ages (Green, 1981) with errors reported in the 95% confidence interval (Brandon, 2002).

## **Results:**

Low-temperature AHe and AFT thermochronometric ages from the steep topographic transect reveal an early to late Miocene cooling history of the Avawatz massif (Tables 1, 2, 3). Apatite He cooling ages from the steep topographic transect were determined for samples A1-A10 using the mean ages of three grains per sample, and are found to span the late Miocene (7.2 – 4.0 ma, Tables 1, 2). Exceptions to the number of multiplets are samples A4, A5, and A10 with which two grains were dated, and sample A3 for which only one grain was dated. The amount of error assigned to mean ages is based on the method of Farley, 2001, using 2-sigma standard error of 11% (Tables 1, 2). For samples with only one grain, or with poor reproducibility, no error is reported. Grains with poor reproducibility include A2-C, A4-B, and A6-C. Inclusion of these grains in calculations of the sample's standard deviation resulted in error values greater than 15%. Samples A1, A4, A5, A6, and A9 from this steep topographic transect have early to middle Miocene AFT cooling ages (19.5 Ma – 9.0 Ma, Tables 1, 2). These are central ages reported with 2-sigma estimates of error. The number of grains dated for these samples range from 10-22, with the exception of sample A5 which only had 6 grains measured (Table 3).

The suite of samples taken across the Mule Spring fault, located 10 km to the west of the steep topographic transect (Figure 2), includes two samples on either side of the Mule Spring fault (four total) that yield both AHe and AFT cooling ages (Figure 7, Tables 1, 4, 5). In addition to this suite of samples, six more AFT cooling ages were determined from samples located within the low foothills, along the range front. Adjacent AFT cooling ages across the fault are found to be mid-late Miocene (~9 Ma) (Figure 7), and the corresponding AHe cooling ages range from latest Miocene to latest Pliocene (5.5 - 2.8 Ma). The four AHe cooling ages are reported as the mean of five grain analyses (Table 5). All error for AHe analyses was determined using the method of Farley (2001) using a standard error of 11%. AHe analyses B3-C, which produces an unusually old cooling age compared to other grains from this sample, was left out for poor reproducibility (Table 5). All AFT cooling ages from the lateral transect have early–middle Miocene cooling ages, with the exception of samples B5, B8, B9 and B10 which have cooling ages spanning the latest Upper Cretaceous to the middle Eocene (72.2 – 42.9 Ma) (Tables 1, 4). These values are reported as central ages with 2-sigma estimates of error. Typically 20 grains were measured to produce AFT ages, with the exception of samples B1, B6, and B10 which utilized fewer than 10 grains (Table 4).

### **Modeling:**

The timing of the exhumational event that produced the Avawatz massif is not obvious from trends in AFT and AHe ages (Figure 9). In order to determine which cooling histories are consistent with our thermochronometric ages, HeFTy 1.8.0.64 (Ketchum, 2005) was used to model data from this study as well as that of Reinert, 2004. Forward modeling with HeFTy can predict cooling ages for various prescribed

time-temperature cooling pathways, allowing one to model what changes in cooling rate, as well as timing of cooling events, can predict a range of measured data (e.g. Clark et al., 2010; Lease et al., 2011; Duvall et al., 2013). To determine whether or not a change in cooling rate is required to explain the spread of measured AHe and AFT ages from Reinert, 2004, a forward model was used to refine the geologic scenarios consistent with the data.

Inverse modeling with HeFTy produces varying cooling pathways that are consistent with model constraints, such as cooling ages and control regions. Control regions were first defined by the AFT and AHe closure temperatures, and age constraints were widened until they did not dictate model outputs. Inverse modeling with HeFTy then randomly generates multiple cooling pathways, recording statistically acceptable and statistically good fits, as well as the best-fit modeled cooling pathway, and the average modeled cooling pathway.

### ***Inverse modeling***

Four samples from across the Mule Spring fault, two in the hanging wall and two in the footwall, were inverse modeled to compare their cooling histories (Figure 10). Each sample has both an AFT and an AHe cooling age, and all are from comparable elevations. Thus, any difference in a samples cooling history should relate to variations in exhumation rates across the fault. Samples B1 and B6 are located south of the Mule Spring fault (Figure 7). Inverse modeling indicates that the best-fit cooling history for sample B1 is one of slow cooling before 11 Ma, followed by an increase in exhumation rate at ~11 Ma (Figure 10). Modeled cooling ages from sample B3, located in the

footwall of the Mule Spring fault across from sample B1, reveals a history of slow cooling before ~12 Ma, followed by an increase in exhumation at 12 Ma, as well as another increase beginning at 3 Ma and continuing to the present (Figure 10). Modeling of sample B6 (Figure 10), located 2 km east of samples B1 and B3 along strike of the Mule Spring fault (Figure 7), indicates an increase in exhumation rate at ~3 Ma. However, the amount of error in the AFT cooling age of sample B6 allows for a multitude of different cooling histories. Inverse modeling of sample B7 indicates that the best fit model is one that involves an increase in exhumation rate at ~ 9 Ma (Figure 10).

### ***Forward Modeling***

Theoretical samples at different depths in a column of rock were prescribed the same cooling history, in 5°C increments over a range of 30°C, representing a ~1 km thick section of rock based on the local measured geothermal gradient of 31.02 +/-0.03 °C/km (Sass et al., 1994). A multitude of different one-stage cooling histories were modeled to see if the observed data fit this simple geologic scenario. After which, two-stage cooling histories were prescribed and modeled to see if a better fit to observed cooling ages could be produced. The simplest prescribed cooling history found to produce modeled cooling ages that are within error of the measured cooling ages is then accepted as the likely geologic scenario.

For initial comparison, when AHe and AFT cooling ages from the hanging wall of the hypothesized fault (Reinert, 2004) are plotted against elevation, the data trends yield apparent exhumation rates of 0.13 km/Ma between 9-15 Ma, and 0.30 km/Ma between 7 and 4 Ma (Figure 9). Because the data do not show a break in slope typical

of an exhumational event, the exhumational event that made the Avawatz is interpreted to have occurred either between the 7-9 Ma gap in AHe and AFT cooling ages, or shortly before. Forward modeling these ages using HeFTy reveals that one-stage cooling models produce ages that are inconsistent with all data points – one-stage cooling rates that match AHe ages produce AFT that are too young (Figure 11), and one-stage rates that match AFT ages produce AHe ages that are too old (Figure 12). Because one-stage cooling models are inadequate in matching the data, two-stage cooling models were then tested and found to produce modeled ages consistent with analyses (Figure 13). Testing which cooling rates match the AHe data reveals that rates must be less than 6.5 °C/Ma (0.21 km/Ma) and greater than 5.5 °C/Ma (0.18 km/Ma) for the last ~10 Ma, or else AHe ages are too young/old, respectively. A multitude of different two-stage cooling models were examined, and the timing of the change in exhumation rate was varied between 11 and 7 Ma. It was observed that any successful two-stage model changed the cooling rate between 9-11 Ma. In the best fitting model the rate doubles during this 9-11 Ma window from a rate of ~3 °C/Ma between ~25 and ~10 Ma, to ~ 6 °C/Ma from ~10 Ma to present (0.1 km/Ma to 0.2 km/Ma exhumation rates, respectively) (Figure 13). It was also found that a long time spent at a low cooling rate of 0.8°C/Ma (0.03 km/Ma) between 50-10 Ma can also produce ages that are consistent with AFT data (Figure 14).

### **Discussion:**

The main contributions of this research are 1) establishing the timing of vertical displacement across the Mule Spring with new thermochronometric ages, and 2) modeling extant data to establish the timing and rate of exhumation of the Avawatz

massif. In doing so, the presence of additional structures has also been identified on both sides of the Mule Spring fault. These findings can then be used to make broader interpretations concerning the structural evolution of the range, as well as relationship between the southern Death Valley and Garlock fault zones.

### ***Vertical displacement across Garlock***

Apatite fission-track cooling ages (~10 Ma) from the western portion of the range do not indicate vertical displacement across the Mule Spring fault since the mid-Miocene. However, AHe ages do indicate vertical displacement, and show an overall eastward increase in offset. Samples B1 and B3 (AHe ages of 5.5 +/- 0.9 Ma, 3.5 +/- 0.7 Ma, respectively) are statistically different ages, with the younger sample B3 located in the footwall of the Mule Spring. Samples B6 and B7 (AHe ages of 2.8 +/- 0.5 Ma, 5.5 +/- 0.9 Ma, respectively) are also statistically different, with the younger sample B6 located in the hanging wall of the Mule Spring fault. These displacements indicate opposing senses of slip – when the cooling ages of samples B1 and B3 are compared (Figure 7), younger ages are in the footwall of the Mule Spring fault, whereas when samples B6 and B7 are compared, younger ages are in the hanging wall. These opposing senses of slip are interpreted to indicate that at this location vertical displacement along strike can be described as a ‘scissor-like’ motion as these two fault zones interact with one another. Alternatively, since the Mule Spring is steeper in this region, these ages may reflect a sub-vertical ‘chattering’ as the Avawatz bump up against the foothills. It is possible that as the Mule Spring fault wraps around the range it becomes increasingly thrust sense. This change in strike may partition left-lateral offset into reverse dip-slip, potentially accounting for why lateral offset decreases

eastwardly. Thus, the fact that the vertical displacement increases to the east is consistent with what one would expect of a strike-slip fault that changes strike to become a thrust, similar to the idea of a compressive restraining bend in other strike-slip fault zones.

Interestingly, when AHe ages from the hanging wall transect in the east of the range are analyzed, there is no indication of vertical displacement across the Mule Spring fault. At this location, ~7 Ma cooling ages are found at equal elevations, on opposing sides of the Mule Spring fault. Either this structure has been mapped incorrectly, or uplift has occurred along additional structures in this portion of the range. Young offset of Holocene alluvial fans does however confirm the sense of slip along this portion of the Mule Spring as thrust-sense, emplacing bedrock over alluvium.

#### ***Presence of additional structure***

Although AHe ages record vertical displacement across the Mule Spring fault in the western portion of the range, there are still very young (i.e., 3.5 +/- 0.7 Ma) ages in the footwall. The presence of young cooling ages in the footwall indicates that another structure(s) may exist along which uplift of the range may have occurred. Examining the AFT cooling ages reveals a bimodal distribution of ages (Figure 15); younger ~10 Ma ages are centered across the fault and extend into the footwall, and older (42.9-72.2 Ma) ages are located in the distal end of the footwall/foothills. One possible structure that may account for a portion of the uplift and exhumation of the Avawatz Mountains and Mule Spring fault may exist along the boundary between these 'young' and 'old' ages. Observations in the field reveal distributed regions of fault gouge (Figures 3, 4)

near this boundary in AFT ages, as well as a change in topographic slope, evidence that supports the existence of such structures. Another potential interpretation of the bimodal distribution of AFT ages is their emplacement via dextral strike-slip along central branches of the southern Death Valley fault zone. One complication with this interpretation is the presence of Tertiary sedimentary units in the Avawatz foothills that are sourced from the nearby Noble Hills – evidence indicating that the Tertiary-present dextral offset is not large enough to emplace the ‘older’ (42.9-72.2 Ma) ages next to the ‘young’ (~10 Ma) ages. The closest source for the Precambrian granitoids of these ‘older’ ages would have to be the Owlshead Mountains; however this evidence would require a greater offset than what is expressed by Tertiary units. A local pegmatite has been dated using K-Ar to 62.4 Ma (e.g., Stamm, 1981; Spencer, 1981); thus another possibility is that the ‘older’ cooling ages are instead crystallization ages were never thermally reset.

AHe ages from across the Mule Spring fault in the vertical transect reveal no vertical displacement (Figure 8). Because this transect crosses the Mule Spring fault where it is thought to be primarily thrust sense, it is a surprise that no vertical displacement is recorded. However, higher up in this transect there is a displacement in AHe cooling ages at ~900 meters elevation, which places a 4.8 +/- 0.5 Ma AHe age above a 7.2 +/- 0.8 Ma age (Figure 8). This age-elevation relationship indicates slip along an unmapped structure (Reinert, 2004). This unmapped structure is interpreted to indicate that slip along the Garlock has at least partially broken back from the structural position of the Mule Spring fault during the evolution of the range, sometime after ~5 Ma. The presence of young (~7 Ma) AHe ages in the footwall of the

hypothesized structure, as well as on both sides of the Mule Spring fault, indicates that a deeper structure may also exist along which the Avawatz massif and its bounding faults may have been uplifted. Deformation of the bajada indicates that this uplift continues into the Quaternary.

Field relations indicate that vertical displacement along contractional structures has continued until at least the Pleistocene. Uplift of the Avawatz foothills has resulted in the folding of Pleistocene alluvial fan and debris flow complexes above blind contractional structures (Menges, 2007). These uplifted foothills have also stranded numerous alluvial fans as strath unconformities as much as 10 meters above the active channel. Within these uplifted fans are numerous thrust faults juxtaposing fans of different grain size against one another (Figure 16). At the base of these foothills bedrock is thrust above alluvium. Excluding intra-fan thrust faulting, contractional structures in the Avawatz may be interpreted two ways: 1) as a series of forward propagating thrust faults, or 2) a series of steep, thick-skinned faults representing the progressive northeastward direction of uplift. Based on the predominantly crystalline nature of bedrock in the foothills, the latter hypothesis is preferred. In both models, the active front of deformation has not moved far over time, and the structures with younger reverse displacement are those more distal to the Avawatz massif, allowing for the cumulative uplift of the range and the Mule Spring fault.

Forward-modeling of cooling ages from the vertical transect indicates that the exhumational event that produced the Avawatz Mountains likely initiated between 11-9 Ma (Figure 13). Previous estimates of the inception age of the Garlock are post-early Miocene (post 17 Ma) (e.g., Smith 1962, Monastero, 1997) with some studies

interpreting a post – 10 Ma inception (e.g., Blythe and Longinotti, 2013; Burbank and Whistler, 1987; Loomis and Burbank, 1988). A recent study by Blythe and Longinotti (2013), which is consistent with the interpreted inception age from this study, utilized AFT thermochronometry and interpreted a ~10 Ma inception of the western portion of the Garlock fault zone in the Tehachapi Mountains. Having the same age of inception on both the eastern and western end of the Garlock could mean that the fault zone either 1) initially ruptured its entire ~260 km length at ~10 Ma, or 2) initially ruptured (pre ~10 Ma) somewhere along what is now the central Garlock, and subsequently grew outwards toward its present points of termination by ~10 Ma. Because large scale strike-slip fault zones typically grow in length over time, the latter hypothesis is preferred.

### ***Garlock is the 'dominant' structure***

Both the Garlock and the southern Death Valley fault zones have Holocene displacements; however the strike of these fault zones indicates that the GFZ is likely the 'dominant' structure, with the resulting rotation of the Mojave Block seemingly pressing into and deflecting the zone of the SDV from the west, which then changes strike, wrapping around the Avawatz Mountains to the southeast (Figure 1). If the SDV were the 'dominant' structure, we would expect to see portions of the Avawatz massif offset dextrally and emplaced to the south of the range; however this is not observed. I therefore interpret that major strike slip of the southern Death Valley fault zone that has displaced bedrock ended before ~10 Ma, and that the Death Valley terrains from the north were juxtaposed with the Avawatz Mountains before the uplift and exhumation of the Mule Spring fault. Thus, comparing cooling ages across the fault should primarily

reveal differences in vertical displacement across the fault, post-cooling, and have lesser influence from paleotopography and strike-slip.

### **Conclusions:**

There is a growing body of evidence in support of a younger inception age for the Garlock fault zone, with recent studies (Blythe et al, 2013; Burbank & Whistler, 1987; Loomis & Burbank, 1988) generally supporting an initiation of slip between 10 and 7 Ma. Modeling of thermochronometric ages from the Avawatz Mountains is in agreement with a younger age of inception, indicated by an increase in cooling rate from  $\sim 3$  °C/Ma to  $\sim 6$  °C/Ma between 11-9 Ma (0.1 km/Ma to 0.2 km/Ma exhumation rates, respectively). The Mule Spring fault has previously been attributed to be the structure responsible for the uplift and exhumation of the Avawatz Mountains; however this research shows that the structural evolution of the range is not that simple. Although there is evidence in AHe ages for young ( $\sim 3$  Ma) vertical slip along the Mule Spring in the west of the range, this structure does not offset  $\sim 7$  Ma cooling ages in the east. Instead, the presence of 'young' cooling ages in the footwall of the Mule Spring fault indicates that additional structures may exist along which the range, as well as the Mule Spring fault, have been uplifted and exhumed. One such structure may exist at the boundary between 'young' and 'old' AFT ages in the foothills, but additional blind structures may exist beneath the expansive bajada. In addition to footwall structure, there is thermochronometric evidence for vertical displacement along a hypothesized structure (Reinert, 2004) in the hanging-wall of the Mule Spring fault.

It turns out that the relationship between Garlock fault zone and crustal shortening in the Avawatz Mountains is more complex than initially thought. Without the

use of thermochronometry, these structures would not have been revealed, aside from their signature during the Quaternary. Apatite fission-track and apatite helium cooling ages from the Avawatz Mountains are overall very young (<10 Ma) and indicate significant exhumation during the Miocene. Uplift and exhumation of the Avawatz Mountains has therefore represented the deformation front from motion along the Garlock fault zone since at least Miocene time, and continues to present.

### **Acknowledgements:**

I would like to thank my advisor, Darrel Cowan, for his continued academic support and friendship. Discussions with him have proven pivotal in my understanding of the Death Valley region as well as the production of the perfect G&T. I would also like to thank Alison Duvall for taking me under her 'thermochronometric-wing', and her relentless support in writing this manuscript. I would also like to thank Chris Menges, USGS, for spending time with me in the field and introducing me to key outcrops. Without these people my academic development, and this research, would not have been the same.

**Figures:**



Figure 1: Satellite image showing the distribution of mountain ranges and fault zones in the study area. The Garlock fault zone (GFZ) and southern Death Valley fault zone (SDV) intersect in the Avawatz Mountains (AM). To the southeast of the Avawatz Mountains are the Silurian Hills (SH) and Holloran Hills (HH). To the northwest of the Avawatz Mountains are the Noble Hills (NH) and Owlshead Mountains (OM). The Avawatz are located at the nexus of three tectonic regimes: the Basin & Range province to the north, the Eastern California Shear Zone to the east, and the strike-slip regime of the Mojave Block to the southwest. Colored lines are from the USGS Quaternary fault database for Google Earth. Top of image is true north.

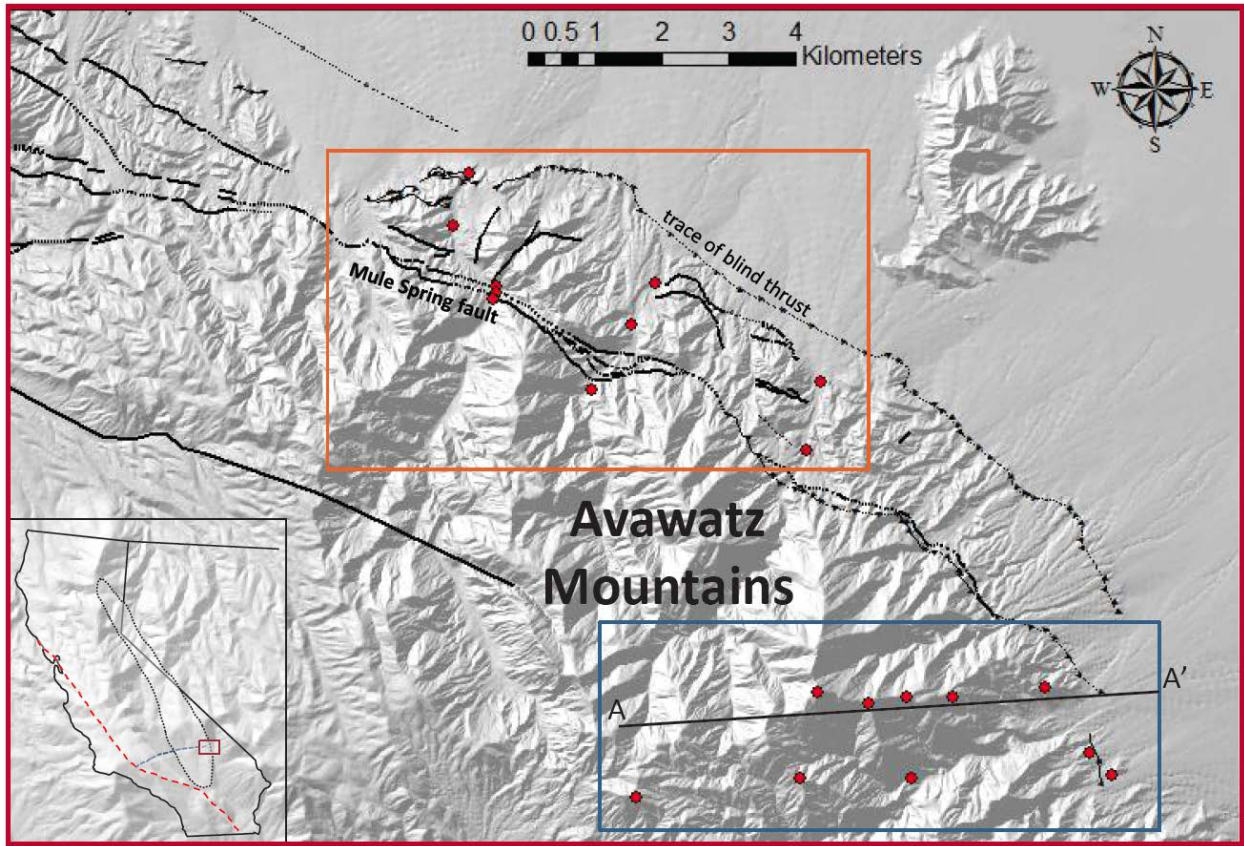


Figure 2: Location of samples (red dots) from across the Mule Spring fault at comparable elevations are outlined in orange (Figure 7). Samples from the steep topographic transect up the hanging wall of the Mule Spring fault are outlined in blue (Figure 5). Inset (bottom left) shows location of figure within southern California, with respect the Garlock fault zone (blue dashed line), San Andreas fault (red dashed line), and Eastern California Shear Zone (black outline). A-A' indicates the map-trace of Figure 6.



Figure 3: Image showing uplifted strath unconformity of the Avawatz foothills – alluvium and debris flow sediment unconformably overlie heavily faulted bedrock. Geologists for scale.



Figure 4: Close up photo of the uplifted strath unconformity of the Avawatz foothills. Much of the bedrock material is heavily faulted, ranging in particle size from gravel to scaly gouge.

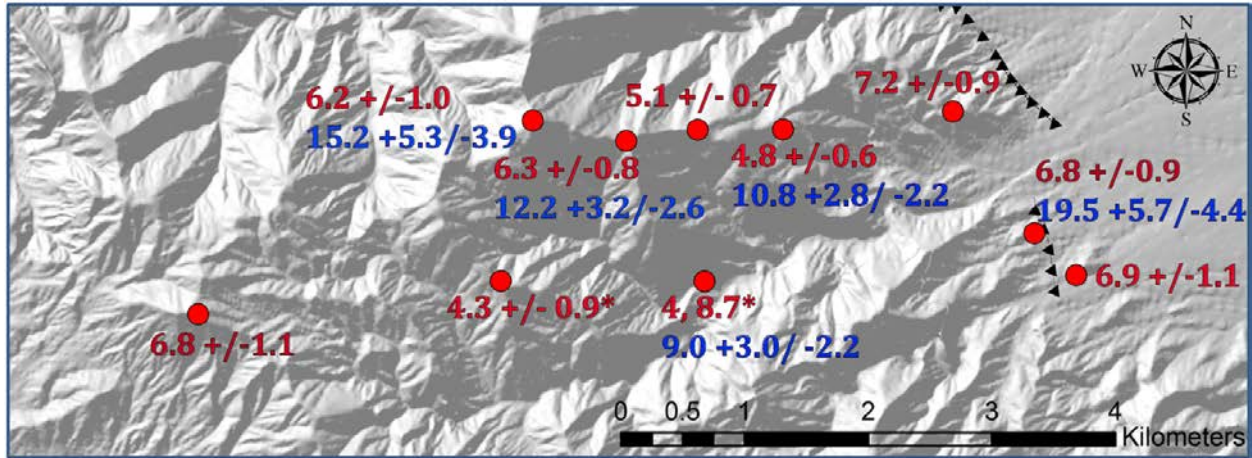


Figure 5: Location of samples from the steep topographic transect up the hanging wall of the Mule Spring fault. Sample locations are shown in red (circles), with AHe (red) and AFT (blue) cooling ages (Ma) for each sample.

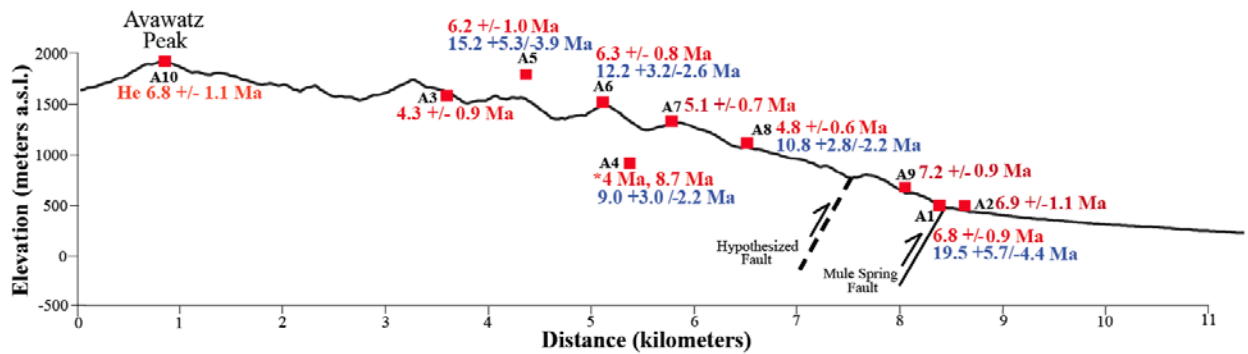


Figure 6: Elevation profile showing the distribution of cooling ages up the steep topographic transect. AHe ages (red) and AFT ages (blue) are in millions of years. Hypothesized fault of Reinert, 2004, shown with the black dashed line, with the Mule Spring fault shown as a solid black line. Map-trace of this transect can be seen as A-A' in Figure 2.

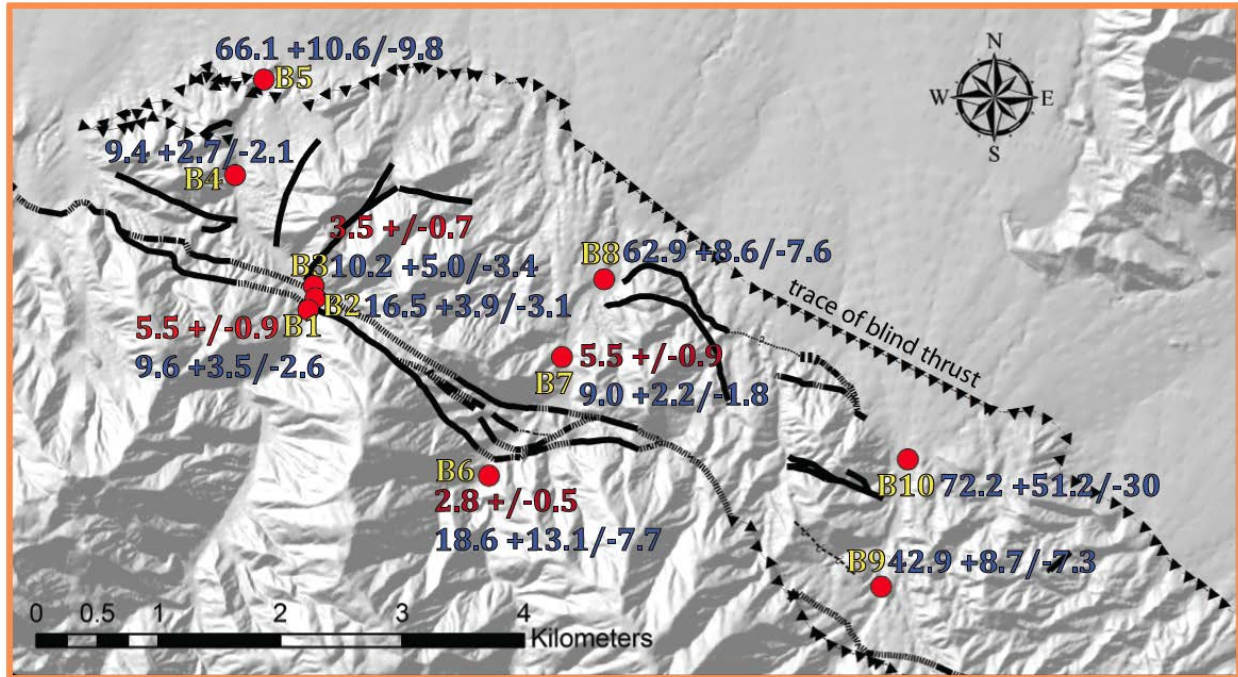


Figure 7: Location of samples taken from across the Mule Spring fault, just east of the Garlock fault zones intersection of the southern Death Valley fault zone. The trace of the blind thrust that has folded Pleistocene alluvial fans can be seen along the northern boundary of the foothills. Sample locations are marked with red circles, with AHe ages (Ma) shown in red, and AFT ages (Ma) shown in blue.

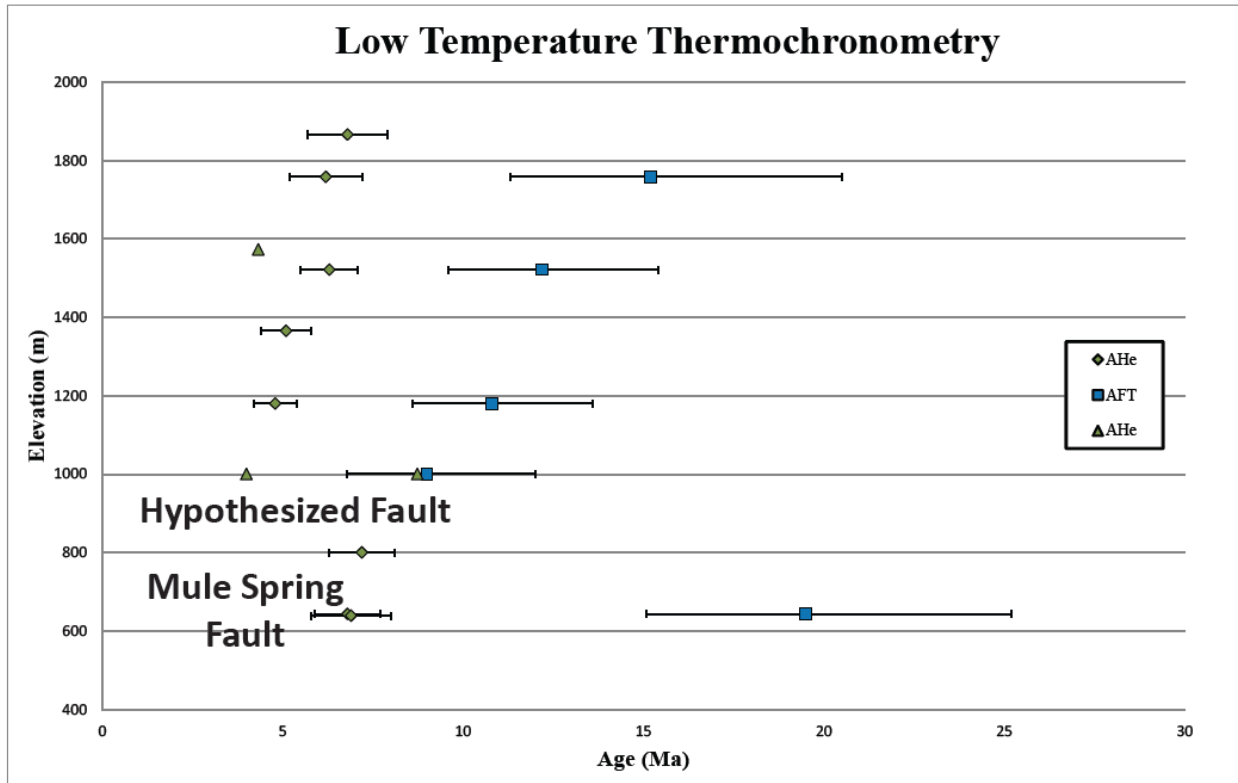


Figure 8: All cooling ages from the hanging wall of the Mule Spring fault. Elevations of structures (Mule Spring fault and hypothesized fault) are shown with text. All AFT (blue squares) and AHe (green diamond) error bars are 2-sigma estimates calculated using the method of Farley, 2001. AHe ages with poor reproducibility or no replicates (green triangles) are shown without error bars.

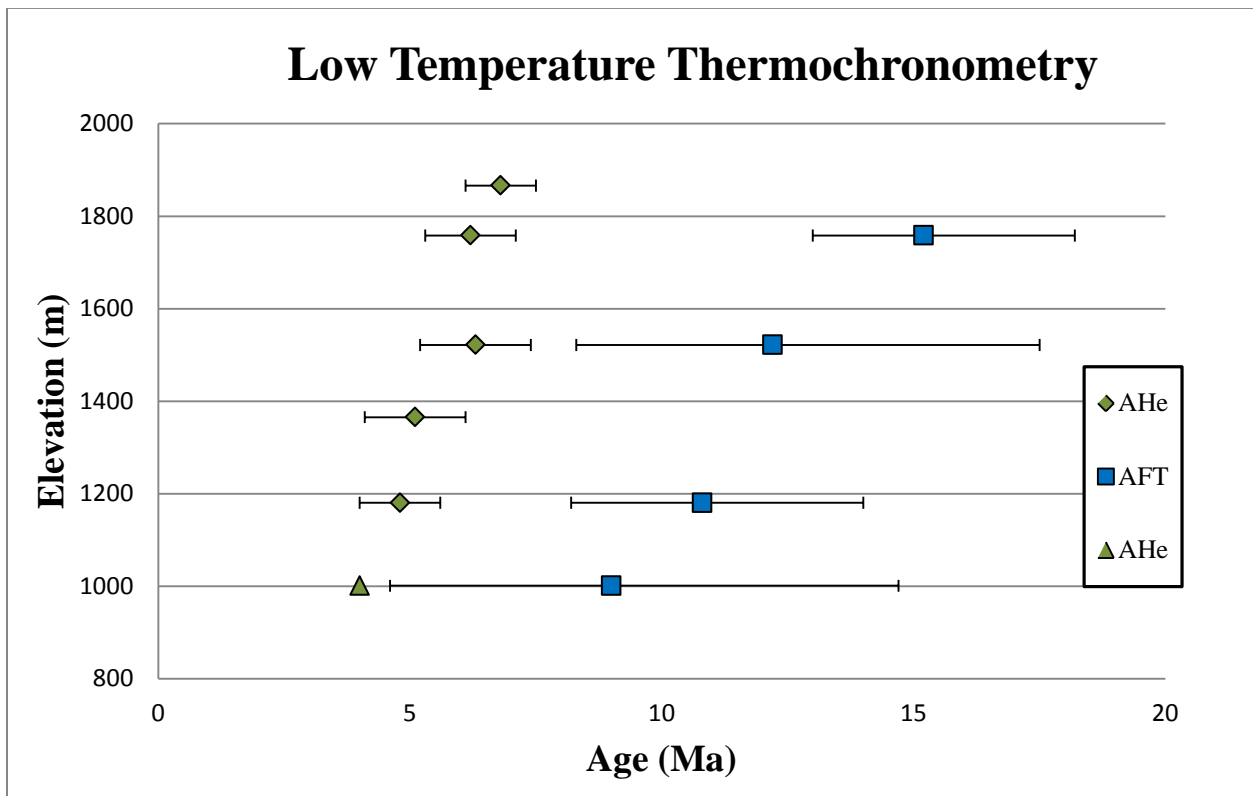


Figure 9: Cooling ages from the hanging wall of the Mule Spring fault, above all known and hypothesized structures. All AFT (blue squares) and AHe (green diamond) error bars are 2-sigma estimates calculated using the method of Farley, 2001. AHe ages with poor reproducibility or no replicates (green triangles) are shown without error bars.

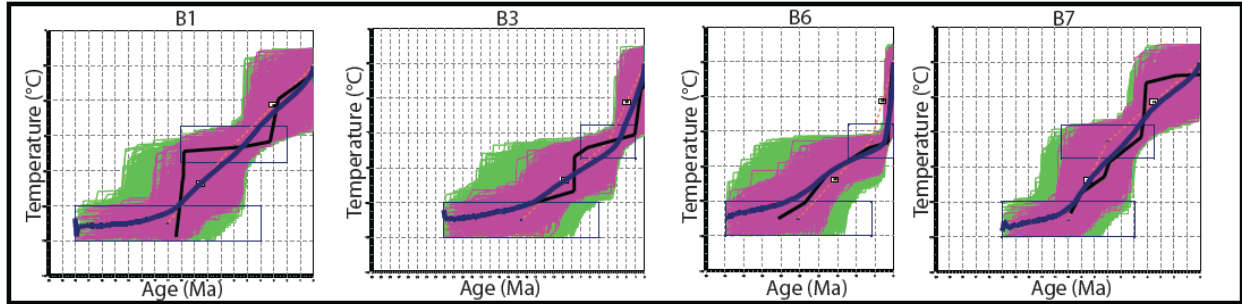


Figure 10: Time-Temperature paths from inverse model results. Samples collected across the Mule Spring fault (B1, B6 in previously mapped hanging wall and B3, B7 in footwall). Green lines indicate cooling pathways of statistically good fit (.5) and Magenta lines indicate regions of acceptable fit (.05). Blue line indicates best fit model. Constraint boxes range across AFT and AHe closure temperatures, age constraints were widened until they no longer dictated modeled pathways.

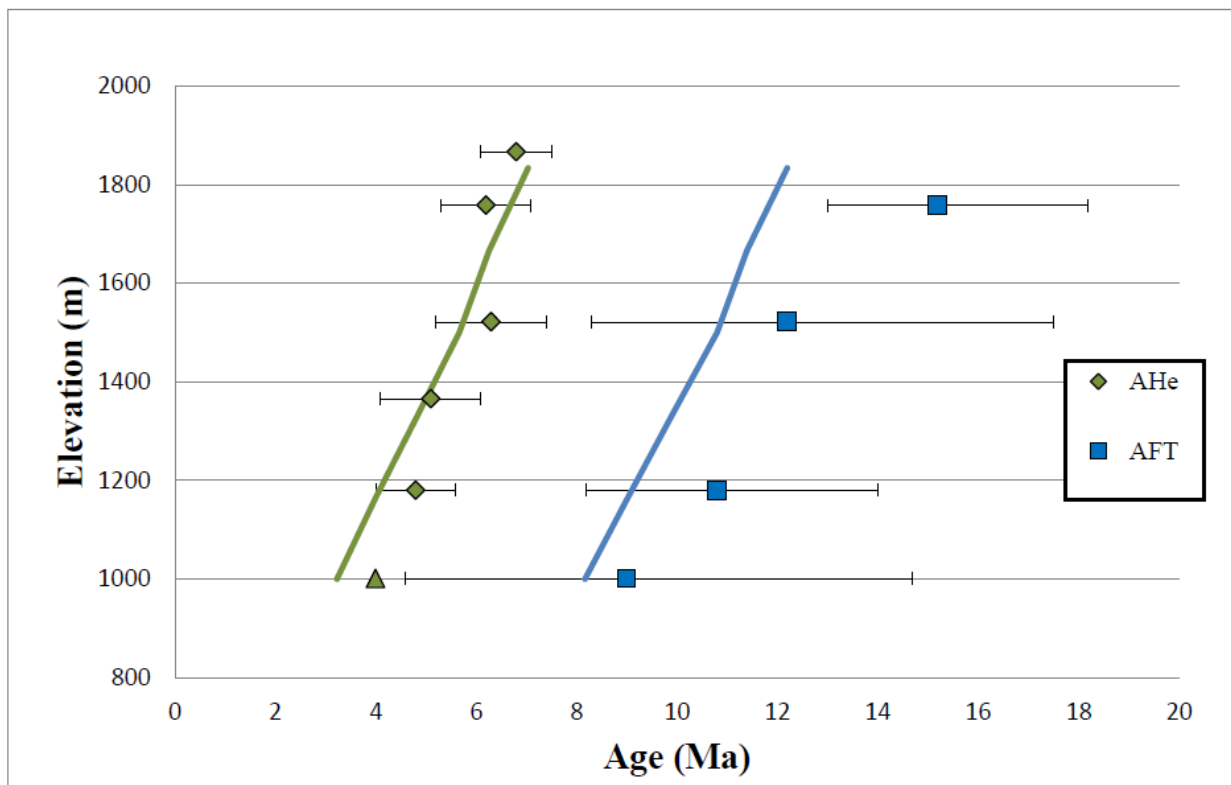


Figure 11: HeFTy forward model output and cooling ages from samples taken above all structure in the hanging wall of the Mule Spring fault. This model assumes one-stage cooling at a rate of 6.25 °C/Ma from 16-0 Ma. Modeled AHe (green line) are consistent with data, yet AFT (blue line) cooling ages are not.

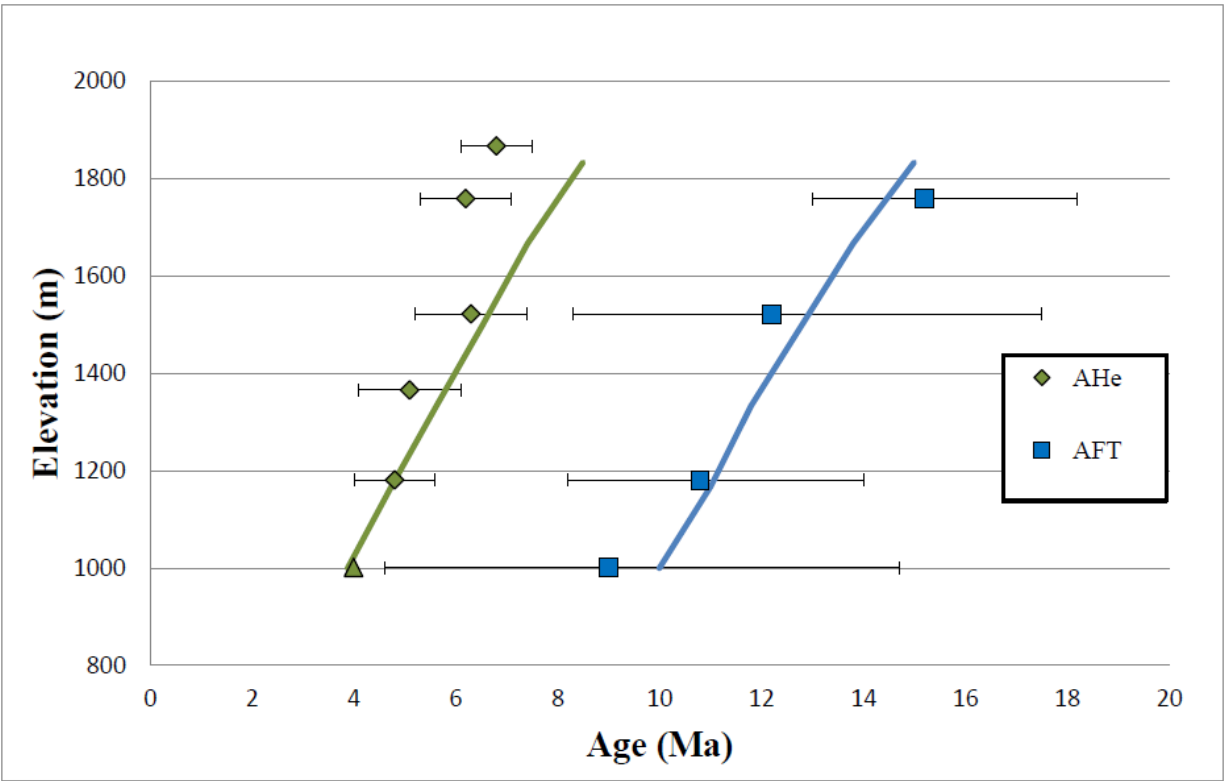


Figure 12: HeFTy forward model output and cooling ages from samples taken above all structure in the hanging wall of the Mule Spring fault. This model assumes one-stage cooling at a rate of 5.0 °C/Ma from 20-0 Ma. Modeled AHe (green line) are inconsistent with data, yet AFT (blue line) cooling ages are consistent.

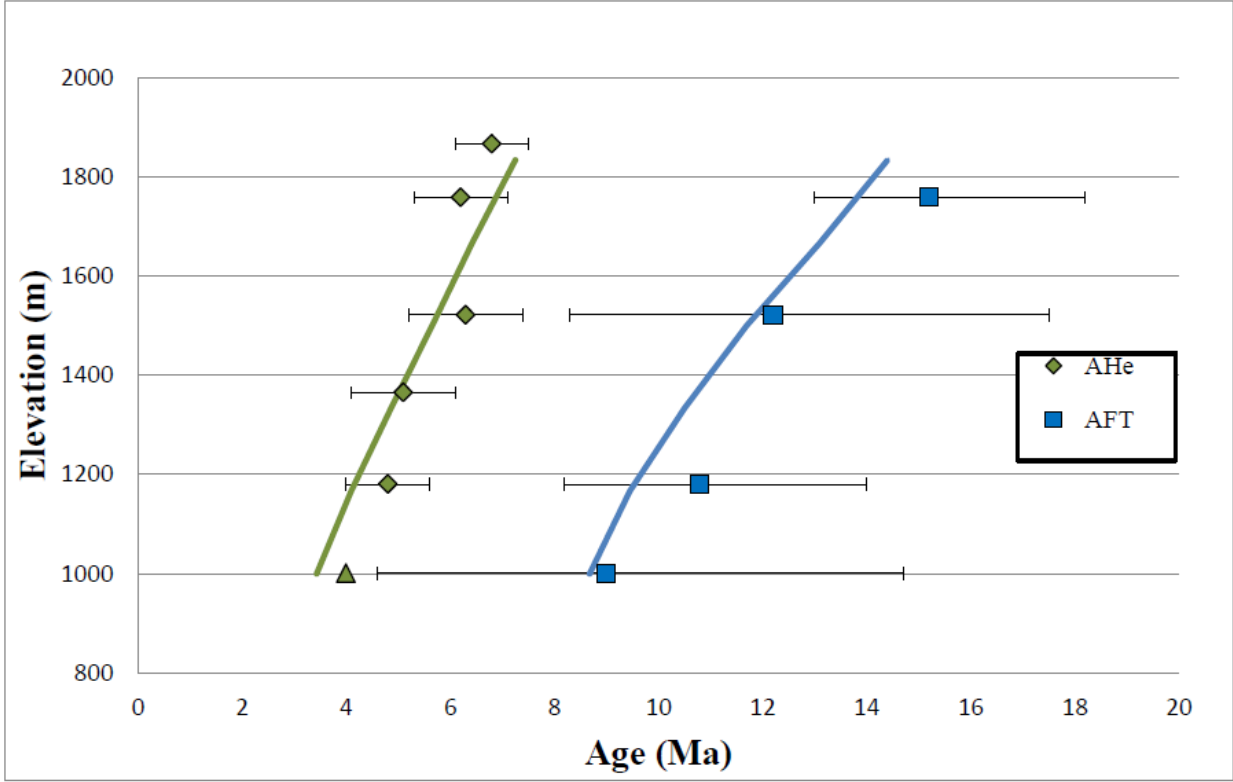


Figure 13: HeFTy forward model output and cooling ages from samples taken above all structure in the hanging wall of the Mule Spring fault. Modeled AHe (green line) and AFT (blue line) cooling ages are consistent with data, and are based on a two-staged cooling history of 3 °C/Ma from 24-10 Ma, followed by 6 °C/Ma from 10-0 Ma.

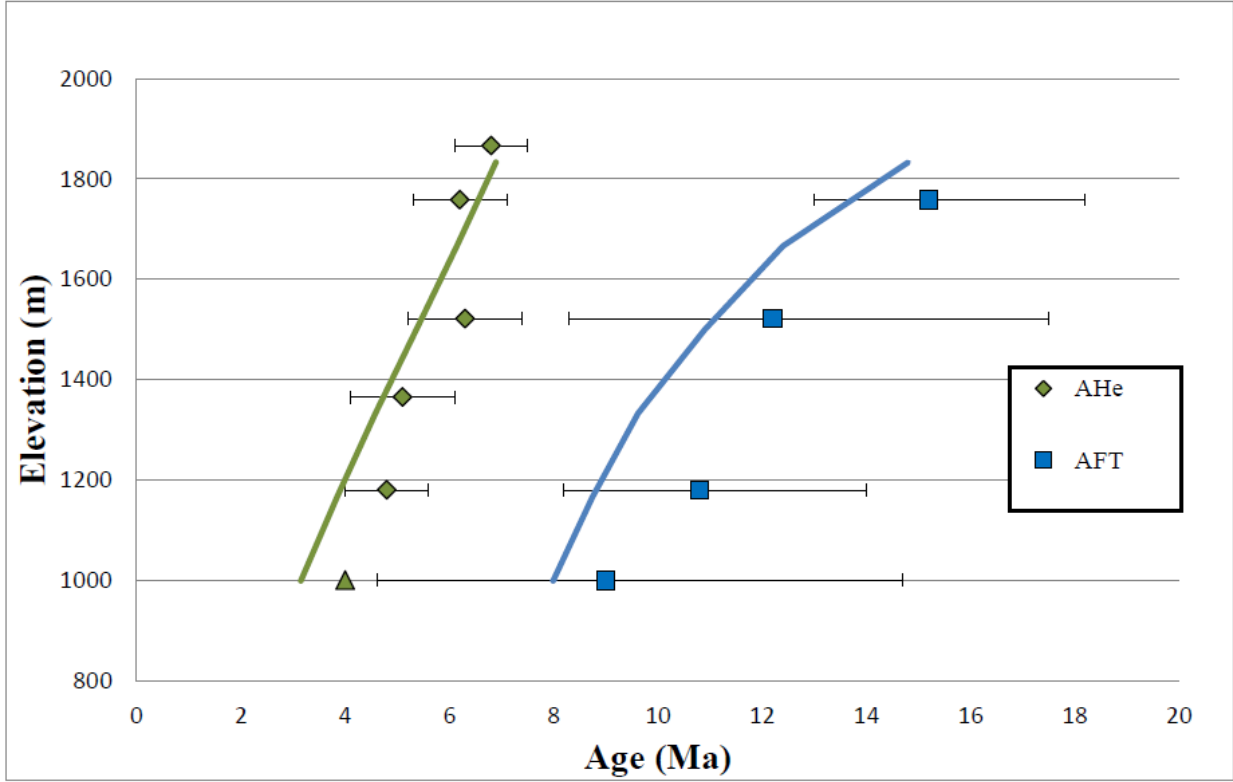


Figure 14: HeFTy forward model output and cooling ages from samples taken above all structure in the hanging wall of the Mule Spring fault. This model assumes two-stage cooling at a rate of 0.77 °C/Ma from 50-11 Ma, followed by a rate of 6.4 °C/Ma from 11-0 Ma. Modeled AHe (green line) and AFT (blue line) cooling ages are consistent with data.

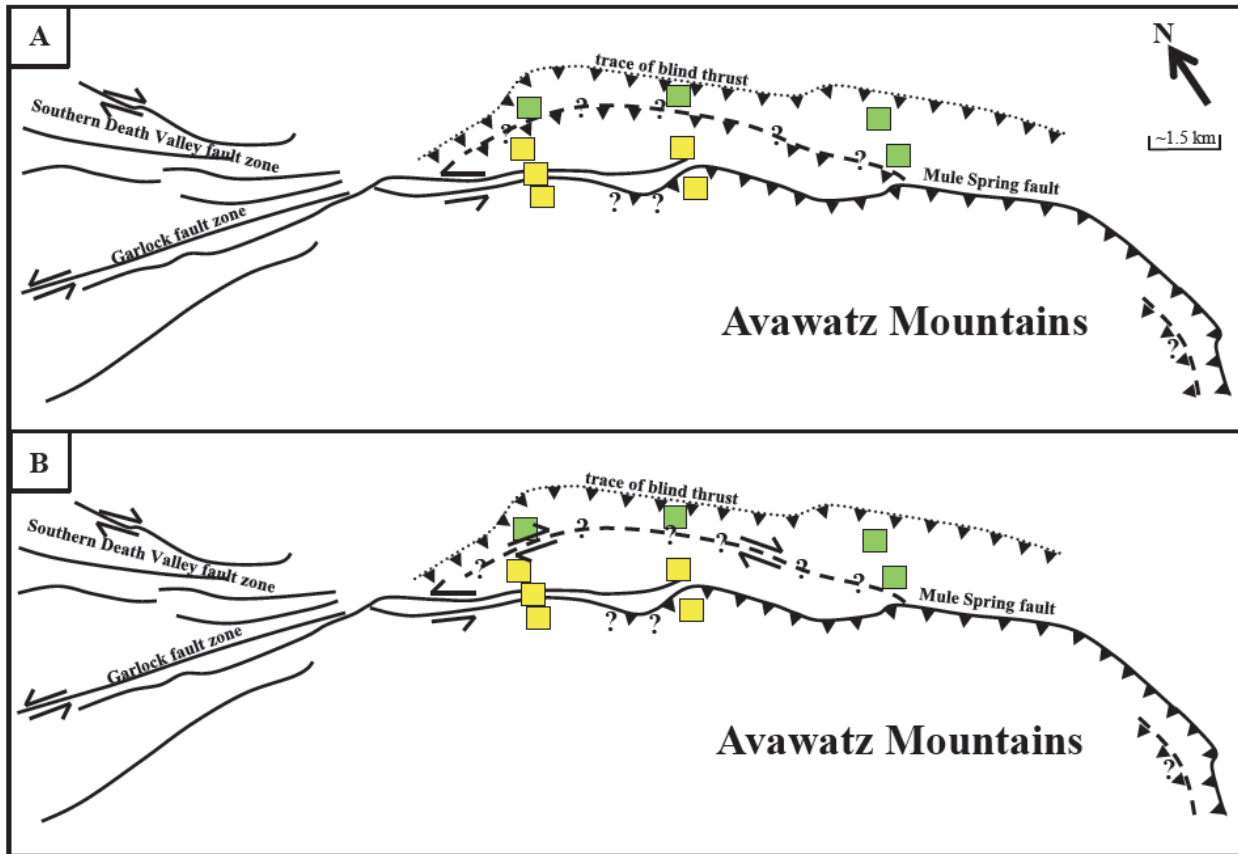


Figure 15: ‘Young’ (~10 Ma) AFT ages from across the Mule Spring fault shown in yellow, with ‘older’ (43-72 Ma) AFT ages shown in green. Section (A) illustrates how the difference in ages may be a result of reverse slip along an unmapped contractional structure. Section (B) illustrates how ‘older’ ages may be juxtaposed with ‘young’ ages by dextral slip of the southern Death Valley fault zone. For actual sample ages, see Figure 7.



Figure 16: Thrust faulting within the alluvial fan and debris flow complexes emplaces fans of different grain size over one another (fault plane to the right of geologist).

Sample	Easting	Northing	Elevation (m)	AHe	AFT
<b>A1</b>	0567452	3930733	650.00	6.8 ( $\pm 0.9$ )	19.5 ( $^{+5.7}/_{-4.4}$ )
<b>A2</b>	0567790	3930392	630.00	6.9 ( $\pm 1.1$ )	
<b>A3</b>	0563134	3930346	1580.00	4.3 ( $\pm 1.0$ )	
<b>A4</b>	0564784	3930344	1010.00	4.0* ( $\pm 1.0$ )	9.0 ( $^{+3.0}/_{-2.2}$ )
<b>A5</b>	0563392	3931647	1761.00	6.2 ( $\pm 1.0$ )	15.2 ( $^{+5.3}/_{-3.9}$ )
<b>A6</b>	0564149	3931483	1524.00	6.3 ( $\pm 0.80$ )	12.2 ( $^{+3.2}/_{-2.6}$ )
<b>A7</b>	0564729	3931574	1365.00	5.1 ( $\pm 0.7$ )	
<b>A8</b>	0565414	3931577	1180.00	4.8 ( $\pm 0.6$ )	10.8 ( $^{+2.8}/_{-2.2}$ )
<b>A9</b>	0566792	3931720	810.00	7.2 ( $\pm 0.9$ )	
<b>A10</b>	0560681	3930076	1850.00	6.82 ( $\pm 1.1$ )	
<b>B1</b>	0558530	3937515	616.16	5.5 ( $\pm 0.9$ )	9.6 ( $^{+3.5}/_{-2.6}$ )
<b>B2</b>	0558587	3937611	620.73		16.5 ( $^{+3.9}/_{-3.1}$ )
<b>B3</b>	0558574	3937711	600.61	3.5 ( $\pm 0.7$ )	10.2 ( $^{+5.0}/_{-3.4}$ )
<b>B4</b>	0557931	3938615	505.49		9.4 ( $^{+2.7}/_{-2.1}$ )
<b>B5</b>	0558167	3939396	493.29		66.1 ( $^{+10.6}/_{-9.8}$ )
<b>B6</b>	0560010	3936161	692.99	2.8 ( $\pm 0.5$ )	18.6 ( $^{+13.1}/_{-7.7}$ )
<b>B7</b>	0560609	3937130	573.17	5.50 ( $\pm 0.9$ )	9.0 ( $^{+2.2}/_{-1.8}$ )
<b>B8</b>	0560955	3937765	511.89		62.9 ( $^{+8.6}/_{-7.6}$ )
<b>B9</b>	0563226	3935254	653.35		42.9 ( $^{+8.7}/_{-7.3}$ )
<b>B10</b>	0563445	3936294	560.98		72.2 ( $^{+51.2}/_{-30}$ )

Table 1: Abbreviated table of AFT and AHe cooling ages.

Sample	UTM Easting (m)	UTM Northing (m)	Elevation (m)	4He (ncc)	[U] (ppm)	[Th] (ppm)	Th/U	He	Mass ( $\mu\text{g}$ )	$F_t$	Radius ( $\mu\text{m}$ )	Age (Ma)	Average Age (Ma)	Error +/- ( $1\sigma$ )	Error +/- ( $2\sigma$ )
<b>A1</b>	0567452	3930733	650												
Analysis a				0.41	110.9	147.3	1.33	90.92	4.53	0.77	60.5	6.74	6.75	0.08	0.17
Analysis b				0.41	154.1	190.4	1.24	129.37	3.14	0.71	42.8	7.62			
Analysis c				0.1	75.3	94.4	1.25	48.58	2.09	0.7	45.8	5.88			
<b>A2</b>	0567790	3930392	630												
Analysis a				0.57	121.3	218.7	1.8	99.98	5.73	0.78	63.8	6.15	6.17	0.14	0.28
Analysis b				0.5	289.9	495.2	1.71	216.45	2.3	0.71	48.5	6.19			
Analysis c				0.86	99.1	156.5	1.58	110.00	7.78	0.80	68	8.41			
<b>A3</b>	0563134	3930346	1580	0.07	98.5	148.7	1.51	45.4	1.48	0.65	36.5	4.33	4.33		
<b>A4</b>	0564784	3930344	1010												
Analysis a				0.02	10.6	5.8	0.55	4.43	5.28	0.77	57.3	4	4		
Analysis b				0.01	5.8	11.1	1.92	5.82	1.72	0.66	37	8.74			
<b>A5</b>	0563392	3931647	1761												
Analysis a				0.14	41.2	28.2	0.69	24.99	5.57	0.77	55.3	5.65	6.19	0.05	0.11
Analysis b				1.12	159.5	198.9	1.25	134.23	8.33	0.8	68.5	6.73			
<b>A6</b>	0564149	3931483	1524												
Analysis a				0.9	119.3	142.9	1.2	102.31	8.76	0.8	68.8	6.9	7.01	0.08	0.15
Analysis b				0.83	136.4	158.7	1.16	118.23	7.05	0.79	66	7.11			
Analysis c				0.12	52.8	66.1	1.25	29.79	4.12	0.75	52.8	4.82			
<b>A7</b>	0564729	3931574	1365												
Analysis a				0.25	139.5	141.1	1.01	78.09	3.23	0.73	47.5	5.16	5.14	0.06	0.13
Analysis b				0.25	138.9	179.3	1.29	81.43	3.04	0.72	47.5	5.15			
Analysis c				0.43	123	147.5	1.2	75.11	5.73	0.77	59.3	5.1			
<b>A8</b>	0565414	3931577	1180												
Analysis a				0.04	25.9	49.6	1.92	15.06	2.92	0.74	57	4.49	4.82	0.12	0.24
Analysis b				0.15	33.1	74.8	2.26	25.85	5.64	0.76	55.5	5.54			
Analysis c				0.27	42.3	112.8	2.67	29.14	9.31	0.79	65	4.41			
<b>A9</b>	0566792	3931720	810												
Analysis a				0.37	107	65.4	0.61	91.65	4.04	0.75	54.5	8.22	7.22	0.04	0.08
Analysis b				0.34	152.8	34.4	0.22	104.45	3.22	0.74	52.5	7.24			
Analysis c				0.24	109.2	58.3	0.53	68.74	3.55	0.75	52.3	6.22			

<b>A10</b>	0560681	3930076	1850												
Analysis a				0.02	16.7	61.3	3.67	14.53	1.4	0.59	29.3	6.56	6.82	0.29	0.57
Analysis b				0.07	38.1	66.9	1.76	32.37	2.15	0.7	46.5	7.08			

Table 2: Apatite helium ages from Reinert 2004.  $F_t$  and radius are mass-weighted values. Ages are correlated for alpha-ejection (Farley et al., 1996). Error values are  $2\sigma$  uncertainties computed using method of Farley et al. (2001).

Sample	UTM Easting (m)	UTM Northing (m)	Elevation (m)	Number of Grains Dated	$\rho_s \times 10^5 \text{ t/cm}^2$	$\rho_l \times 10^6 \text{ t/cm}^2$	$\rho_d \times 10^6 \text{ t/cm}^2$	Central Age, Ma (1 SE)	95%CI (+)	95% CI (-)	$P(\chi)^2 \%$	Uranium Content (SE), ppm
<b>A1</b>	0567452	3930733	650	10	7.79 (125)	3.92 (629)	2.93 (5465)	19.5	5.7	4.4	44.3	53 (5)
<b>A4</b>	0564784	3930344	1010	16	0.57 (77)	0.615 (830)	2.89 (5465)	9	3	2.2	68.9	8 (1)
<b>A5</b>	0563392	3931647	1761	6	6.31 (126)	4.42 (882)	2.87 (5465)	15.2	5.3	3.9	8.1	61 (4)
<b>A6</b>	0564149	3931483	1524	18	4.77 (201)	3.89 (1640)	2.84 (5465)	12.2	3.2	2.6	10.4	55 (3)
<b>A8</b>	0565414	3931577	1180	22	1.22 (198)	1.08 (1743)	2.82 (5465)	10.8	2.8	2.2	8.6	15 (1)

Table 3: Apatite fission track ages from Reinert, 2004. Zeta value is  $67.04 \pm 5.40$

Sample Label	E-W	N-S	Elevation (ft)	Elevation (m)	Quality	Grains Counted	Dose (x10 <sup>6</sup> N/cm <sup>2</sup> s)	Ts	Ti	Central Age (95% CI)	95%CI (+)	95% CI (-)	Chi <sup>2</sup> (%)	DPAR
B1	0558530	3937515	2021	616.2	Poor-inclusions	9	1.15	45	973	9.6	3.5	2.6	96.6	1.93
B2	0558587	3937611	2036	620.7	Fair	20	1.16	108	1377	16.5	3.9	3.1	99.0	1.89
B3	0558574	3937711	1970	600.6	Good	20	1.16	26	537	10.2	5	3.4	100.0	1.72
B4	0557931	3938615	1658	505.5	Good	20	1.17	69	1552	9.4	2.7	2.1	99.7	1.88
B5	0558167	3939396	1455	443.6	Poor	20	1.15	525	1638	66.1	10.6	9.8	7.5	1.95
B6	0560010	3936161	2273	693.0	Poor- tiny	9	1.17	15	171	18.6	13.1	7.7	100.0	1.7
B7	0560609	3937130	1880	573.2	Great	20	1.19	99	2363	9	2.2	1.8	100.0	1.93
B8	0560955	3937765	1679	511.9	Great	20	1.19	497	1698	62.9	8.6	7.6	87.6	1.79
B9	0563226	3935254	2143	653.4	Good	20	1.20	166	839	42.9	8.7	7.3	84.3	1.96
B10	0563445	3936294	1840	561.0	Poor	5	1.20	18	54	72.2	51.2	30	99.3	1.88

Table 4: Apatite fission-track ages from across the Mule Spring fault, near the Garlock fault zone's intersection with the southern Death Valley fault zone. Zeta: 363 +/- 14

							Dimensional Mass					Mass Independent Abundances											
Full Sample Name	length 1 (μm)	width 1 (μm)	length 2 (μm)	width 2 (μm)	2X Term	Dim Mass (μg)	4He (nmol/g)	U (ppm)	Th (ppm)	Sm (ppm)	eU	rs (μm)	4He (ncc)	U (ng)	Th (ng)	Sm (ng)	Raw Date (Ma)	Ft	Corrected Date (Ma)	Total Mean Corrected Age	Selected Mean Age (Ma)	Error +/- (1σ)	Error +/- (2σ)
B1_A*	217.4	88.2	211.2	65.9	N	2.64	1.717	76.27	46.92	13.52	87.3	48.98	0.102	0.2017	0.1241	0.0357	3.64	0.684	5.33	5.46	5.46	0.45	0.90
B1_B	151.9	85.0	145.1	74.7	N	1.97	3.927	182.21	67.40	21.32	198.1	47.20	0.173	0.3586	0.1326	0.0420	3.67	0.683	5.38				
B1_C	155.7	115.3	158.5	95.3	N	3.62	1.150	47.22	28.82	8.74	54.0	59.15	0.093	0.1710	0.1043	0.0316	3.94	0.744	5.30				
B1_D	157.6	99.0	158.9	70.2	Y	2.35	5.137	216.05	168.15	24.43	255.6	50.07	0.271	0.5086	0.3959	0.0575	3.72	0.677	5.49				
B1_E	185.1	140.2	189.2	100.4	N	5.63	1.125	41.10	22.79	6.87	46.5	68.28	0.142	0.2314	0.1283	0.0387	4.49	0.775	5.78				
B3_A*	147.4	121.5	145.8	89.0	Y	3.38	0.199	14.34	21.74	18.89	19.4	58.09	0.015	0.0484	0.0734	0.0638	1.88	0.717	2.62	4.12	3.52	0.33	0.66
B3_B	188.2	85.5	189.1	77.5	Y	2.60	0.255	10.67	20.71	16.67	15.5	50.27	0.015	0.0278	0.0539	0.0434	3.01	0.671	4.49				
B3_C	116.0	99.2	116.0	85.9	N	2.07	0.219	5.58	13.83	12.64	8.8	49.62	0.010	0.0115	0.0286	0.0261	4.53	0.695	6.51				
B3_D	163.1	78.8	159.7	69.6	Y	1.85	0.309	19.04	37.28	19.17	27.8	45.25	0.013	0.0352	0.0689	0.0354	2.05	0.640	3.20				
B3_E	108.3	78.3	108.8	78.9	Y	1.39	0.877	51.71	70.46	39.91	68.3	43.28	0.027	0.0721	0.0982	0.0556	2.37	0.631	3.75				
B6_A*	122.6	73.5	123.7	60.4	N	1.15	0.224	14.03	28.25	5.11	20.7	39.48	0.006	0.0161	0.0324	0.0059	2.01	0.617	3.25	2.81	2.81	0.23	0.46
B6_B	138.1	117.4	138.1	105.3	N	3.56	0.326	18.45	51.91	5.52	30.6	59.52	0.026	0.0657	0.1848	0.0196	1.97	0.741	2.65				
B6_C	112.4	74.2	112.4	65.5	N	1.14	0.372	20.88	72.46	7.16	37.9	39.97	0.010	0.0238	0.0826	0.0082	1.81	0.619	2.93				
B6_D	150.5	78.9	148.3	56.2	N	1.42	0.127	11.09	21.88	3.05	16.2	41.32	0.004	0.0157	0.0310	0.0043	1.45	0.628	2.30				
B6_E	106.5	91.8	116.2	66.6	N	1.45	0.394	20.82	75.36	8.37	38.5	43.82	0.013	0.0302	0.1094	0.0122	1.89	0.649	2.91				
B7_A**	131.2	103.8	128.8	78.4	Y	2.24	0.880	42.92	5.00	32.38	44.1	50.72	0.0443	0.0963	0.0112	0.0726	3.68	0.688	5.35	5.50	5.50	0.45	0.90
B7_B	105.5	69.3	107.9	57.0	N	0.88	1.487	75.20	16.57	44.92	79.1	36.45	0.0295	0.0665	0.0147	0.0397	3.47	0.605	5.74				
B7_C	108.0	70.0	108.1	62.9	N	0.99	0.917	53.82	17.78	31.60	58.0	38.11	0.0204	0.0534	0.0176	0.0313	2.92	0.620	4.71				
B7_D	103.9	70.4	105.2	57.7	N	0.89	0.559	34.84	29.22	30.38	41.7	36.72	0.0112	0.0311	0.0260	0.0271	2.47	0.603	4.10				
B7_E	168.1	71.8	166.8	58.3	Y	1.47	2.379	87.40	27.97	49.04	94.0	40.88	0.0785	0.1287	0.0412	0.0722	4.68	0.616	7.59				

\*Average Durango Age Standard for this run  
 $31 \pm 2.7$  Ma (n=34)  
\*\*Average Durango Age Standard for this run  
 $30.88 \pm 1.19$  Ma (n=6)

Table 5: Apatite helium ages from across the Mule Spring fault. Error values are 2σ uncertainties computed using method of Farley et al. (2001).

## **References:**

Blythe, A., Longinotti, N., 2013, Exhumation of the southern Sierra Nevada - eastern Tehachapi Mountains constrained by low-temperature thermochronology: Implications for the initiation of the Garlock fault, *Lithosphere*, v. 5, p. 321-327.

Brandon, M., 2002, Decomposition of mixed grain-age distributions using BINOMFIT: *On Track*, v. 24, p. 13–18.

Brady, R., Troxel, B., 1981, Eastern termination of the Garlock fault in the Avawatz Mountains, San Bernardino County, California. *Geological Society of America Abstracts with Programs*, v. 13, p. 46-47.

Brady III, R., 1984, Neogene stratigraphy of the Avawatz Mountains between the Garlock and Death Valley fault zones, southern Death Valley, California: Implications as to Late Cenozoic tectonism, *Sedimentary Geology*, v. 38, p. 127-157.

Brady III, R., 1986, Stratigraphy and tectonics of the northern Avawatz Mountains at the intersection of the Garlock and Death Valley fault zones, San Bernardino County, California. *Quaternary tectonics of southern Death Valley, California—Field trip guide: Shoshone, California, Friends of the Pleistocene, Pacific Cell*, p. 1-12.

Brady III, R., 1988, Southward continuation of the southern Death Valley fault zone from the Avawatz Mountains to the Bristol Mountains, San Bernardino County, California: *Geological Society of America Abstracts with Programs*, v. 20, no. 3, p. 145.

Bryant, W., compiler, 2000, Fault number 69a, Garlock fault zone, Western Garlock section, in *Quaternary fault and fold database of the United States*: U.S. Geological Survey website, <http://earthquakes.usgs.gov/regional/qfaults>

Burbank, D., Whistler, D., 1987, Temporally constrained tectonic rotations derived from magnetostratigraphic data: Implications for the initiation of the Garlock fault, California: *Geology*, v. 15, p. 1172-1175.

Burchfiel, B., Stewart, J., 1966, "Pull-apart" origin of the central segment of Death Valley, California. *Geological Society of America Bulletin*, v. 77, no. 4, p. 439-442.

Butler, P., 1984, *Geology, structural history, and fluvial geomorphology of the southern Death Valley fault zone, Inyo and San Bernardino Counties, California*: Davis, University of California, unpublished Ph.D. dissertation, 122 p., 2 pls., scale 1:24,000.

Calzia, J., and Rämö, O., 2000, Late Cenozoic crustal extension and magmatism, southern Death Valley region, California, *in* Lageson, D.R., and others, eds., *Great Basin and Sierra Nevada: Boulder, Colorado, Geological Society of America field Guide 2*, p. 135-164.

Clark, M., Farley, K., Zheng, D., Wang, Z., Duvall, A., 2010, Early Cenozoic faulting of the northern Tibetan Plateau margin from apatite (U-Th)/He ages, *Earth and Planetary Science Letters*, v. 296, p 78-88

Davis, G., Burchfiel, B., 1973, Garlock fault: An intracontinental transform structure, southern California: *Geological Society of America Bulletin*, v. 84, p. 1407-1422.

Dodson, M., 1973, Closure temperature in cooling geochronological and petrological systems, *Contribution to Mineralogy and Petrology*, v. 40, p. 259–274.

Duvall, A., Clark, M., Kirby, E., Farley, K., Craddock, C., Dao-Yang, Y., 2013, Low-temperature thermochronometry along the Kunlun and Haiyuan Faults, NE Tibetan Plateau: Evidence for kinematic change during late-stage orogenesis, *Tectonics*, v. 32, no. 5, p. 1190-1211.

Ehlers, T., Willett, S., Armstrong, P., Chapman, D., 2002, Exhumation of the central Wasatch Mountains, Utah: 2. Thermo-kinematic model of exhumation, erosion, and thermochronometer interpretation, *Journal of Geophysical Research*, v. 108, no. B3, p. 2173.

Farley, K., Rusmore, M., Bogue, S., 2001, Post-10 Ma uplift and exhumation of the Northern Coast Mountains, British Columbia, *Geology*, v. 29, p. 99-102.

Farley, K., 2000, Helium diffusion from apatite: General behavior as illustrated by Durango fluorapatite, *Journal of Geophysical Research*, v. 105, p. 2903–2914.

Farley, K., Wolf, R., Silver, L., 1996, The effects of long alpha-stopping distances on (U-Th)/He ages, *Geochim. Cosmochim. Acta*, v. 60, p. 4,223–4,229.

Fleischer, R., Price, P., Walker, R., 1975, *Nuclear Tracks in Solids*, Berkeley: University of California Press, 605 p.

Flowers, R., Ketcham, R., Shuster, D., Farley, K., 2009, Apatite (U-Th)/He thermochronometry using a radiation damage accumulation and annealing model, *Geochim. Cosmochim. Acta*, v. 73, no. 8, p. 2347–2365.

Gleadow, A., Duddy, I., 1981, A natural long-term track annealing experiment for apatite, *Nucl. Tracks*, v. 5, p. 169–174.

Green, P., 1981, A new look at statistics in fission track dating: *Nuclear Tracks*, v. 5, p. 77–86.

Green, H., Redwine, J., Miller, D., 2007, Reconnaissance studies of soils; geomorphic correlations and late Quaternary deformation of alluvial fan deposits east of the Avawatz Mountains, Mojave Desert, California. *in* Miller, D., Valin, Z., eds, 2007, *Geomorphology and tectonics at the intersection of Silurian and Death Valleys, southern California—2005 Guidebook*, Pacific Cell Friends of the Pleistocene: U.S. Geological Survey Open-File Report 2007–1424, p. 113-139.

Ketcham, R., 2005, Forward and inverse modeling of low-temperature thermochronometry data, *in* Reiners, P., and Ehlers, T., eds., *Low-Temperature Thermochronology: Reviews in Mineralogy and Geochemistry*, v. 58, p. 275–314.

Ketcham, R., Carter A., Donelick, R., Barbarand, J., Hurford, A., 2007, Improved modeling of fission-track annealing in apatite. *Am. Mineral.*, v. 92, p. 799–810.

Lease, R., Burbank, D., Clark, M., Farley, K., Zheng, D., Zhang, H., 2011, Middle Miocene reorganization of deformation along the northeastern Tibetan Plateau, *Geology*, v. 39, p. 359–362.

Loomis, D., Burbank, W., 1988, The stratigraphic evolution of the El Paso basin, southern California: Implications for the Miocene development of the Garlock fault and uplift of the Sierra Nevada, *Geological Society of America Bulletin*, v. 100, no. 1, p. 12-28

Machette, M., Piety, L., compilers, 2001, Fault number 143b, Southern Death Valley fault zone, Nobel Hills section, in *Quaternary fault and fold database of the United States: U.S. Geological Survey website*, <http://earthquakes.usgs.gov/hazards/qfaults>, accessed 12/05/2013.

McGill, S., Sieh, K., 1991, Surficial offsets on the central and eastern Garlock fault associated with prehistoric earthquakes. *Journal of Geophysical Research*, v. 96, p. 21597-21621.

Mendonça, J., 2006, Neotectonic evolution of the Avawatz Mountains, southern Death Valley, California, Masters thesis, San Jose State University, 88 p.

Mendonça, J., 2007, Preliminary results on neotectonic and geomorphic evolution of the northeastern Avawatz Mountains, southern Death Valley, California. *in* Miller, D., Valin, Z., eds., 2007, *Geomorphology and tectonics at the intersection of Silurian and Death Valleys, southern California—2005 Guidebook*, Pacific Cell Friends of the Pleistocene: U.S. Geological Survey Open-File Report 2007–1424, p. 141-148.

Menges, C., Pavlis, T., McMackin, M., Serpa, L., Bennett, R., 2005, Geomorphic and structural evidence for significant neotectonic contractional strain within southern Death Valley and bordering areas, eastern California. *Geological Society of America Abstracts with Programs*, v. 37, no. 7, p. 69.

Menges, C., 2007, Geomorphology and tectonics at the intersection of Silurian and Death Valleys, southern California, *Pacific Cell Friends of the Pleistocene Guidebook*, USGS Open-File Report, 1424, p. 21-49

Monastero, F., Sabin, A., Walker, J., 1997, Evidence for post-early Miocene initiation of movement on the Garlock fault from offset of the Cudahy Camp Formation, east-central California, *Geology*, v. 25, no. 3, p. 247-250.

Noble, L., 1941, Structural features of the Virgin Spring area, Death Valley, California: Geological Society of America Bulletin, v. 52, p. 941-1000.

Piety, L., 1995, Compilation of known and suspected Quaternary faults within 100 km of Yucca Mountain, Nevada and California: U.S. Geological Survey Open-File Report 94-112, 404 p., 2 pls., scale 1:250,000.

Reiners, P., Brandon, M., 2006, Using Thermochronology to Understand Orogenic Erosion, Annual Review of Earth and Planetary Science, v. 34, p. 419-66

Reinert, E., 2004, Low-temperature thermochronometry of the Avawatz Mountains, California: Implications for the inception of the Eastern California Shear Zone, University of Washington Master's Thesis, 31 p.

Sass, J., Pries, S., Lachenbruch, A., Moses Jr., T., Galanis J.r., S., Munroe, R., Morgan, P., 1994, Thermal regime of the southern Basin and Range Province: 1. Heat flow data from Arizona and the Mojave Desert of California and Nevada, Journal of Geophysical Research, v. 99, no. B11, p. 22,093-22,119.

Shuster, D., Farley, K., 2009, The influence of artificial radiation damage and thermal annealing on helium diffusion kinetics in apatite, Geochimica et Cosmochimica Acta, v. 73, no. 1, p. 183-196.

Smith, G., 1962, Large lateral displacement on Garlock fault, California, as measured from offset dike swarm: American Association of Petroleum Geologists Bulletin, v. 46, p. 85-104.

Smith, G., Ketner, K., 1970, Lateral displacement on the Garlock fault, southeastern California, suggested by offset sections of similar metasedimentary rocks: U.S. Geological Survey Professional Paper 700-D, p. 1-9.

Smith, E., Sanchez, A., Keenan, D., Monastero, F., 2002, Stratigraphy and geochemistry of volcanic rocks in the Lava mountains, California: Implications for the Miocene development of the Garlock fault, in Glazner, A., Walker, J., Bartley, J., eds., Geologic Evolution of the Mojave Desert and Southwestern Basin and Range; Boulder, Colorado, Geological Society of America memoir 195, p. 151-160.

Spencer, J., 1990a, Late Cenozoic extensional and compressional tectonism in the southern and western Avawatz Mountains, southeastern California, in Wernicke, B., ed., Basin and Range extensional tectonics near the latitude of Las Vegas, Nevada; Boulder, Colorado, Geologic Society of America Memoir 176.

Spencer, J., 1990b, Geologic map of Southern Avawatz Mountains, northeastern Mojave Desert region, San Bernardino County, California: U.S. Geologic Survey, miscellaneous field studies map MF-2117.

Spencer, J., 1981, Geology and Geochronology of the Avawatz Mountains, San Bernardino County, California, Massachusetts Institute of Technology, Cambridge, Massachusetts, Ph.D. thesis, 183 p.

Stamm, J., 1981, Geology at the intersection of the Death Valley and Garlock fault zones, southern Death Valley, California, Pennsylvania State University, Ph.D. thesis, 123 p.

Stockli, D., Farley, K., Dumitru, T., 2000, Calibration of the (U-Th)/He thermochronometer on an exhumed fault block, White Mountains, California, *Geology*, v. 28, p. 983-986.

Stroud, J., McGill, S., 1994a, Neotectonic activity on a thrust fault in the northeastern Avawatz Mountains, California: Geological Society of America Abstracts with Programs, v. 26, no. 2, p. 97.

Stroud, J., McGill, S., 1994b, Late Quaternary activity on a thrust fault in the northeastern Avawatz Mountains, Mojave Desert, California: San Bernardino County Museum Association Quarterly, v. 41, no. 3, p. 30-31.

Troxel, B., Wright, L., Jahns, R., 1972, Evidence for differential displacement along the Garlock fault zone, California: Geological Society of America Abstracts with Programs, v. 5, p. 250.

Troxel, B., Butler, P., 1998, Tertiary and Quaternary fault history of the intersection of the Garlock and Death Valley fault zones, southern Death Valley, California, in Calzia, J., Reynolds, R., eds., *Finding Faults in the Mojave: San Bernardino County Museum Association Quarterly*, v. 45, p. 91-98.

Wagner, G., Van den Haute, P., 1992, *Fission track dating*, Kluwer Academic Publishers, 285 p.

Wolf, R., Farley, K., Silver, L., 1996, Helium diffusion and low-temperature thermochronometry of apatite, *Geochimica et Cosmochimica Acta*, v. 60, no. 21, p. 4231-4240.

Warnock, A., Zeitler, P., Wolf, R., Bergman, S., 1997, An evaluation of low-temperature apatite U-Th/He Thermochronometry, *Geochimica et Cosmochimica Acta*, v. 61, no. 24, p. 5371-5377.

Wills, C., Hart, E., Bryant, W., Treiman, J., Kahle, J., 1989, Summary report - Fault evaluation program, 1987-1988, southwestern Basin and Range region and supplemental areas: California Division of Mines and Geology Open-File Report 89-16, 31 p., 1 pl., scale 1:500,000

Zeitler, P., Herczig, A., McDougall, I., Honda, M., 1987, U-Th/He dating of apatite: a potential thermochronometer, *Geochim. Cosmochim. Acta*, v. 51, p. 2865-2868.